The Canadian Mineralogist
Vol. 37, pp. 415-429 (1999)

FORWARD MODELING OF METAMORPHIC TEXTURES

C. THOMAS FOSTER, JR.[1]

Department of Geology, University of Iowa, Iowa City, Iowa 52242, U.S.A.

ABSTRACT

A technique of quantitative forward modeling that combines differential and irreversible thermodynamic relations is used to gain insight into the types of textures that develop in regional metamorphic terranes. Two different P–T paths are examined that produce sillimanite–garnet schist from staurolite–garnet schist of the same bulk composition. One is an isobaric heating path from 600°C to 630°C at 4 kbar, and the other is an isothermal decompression path from 8 kbar to 4 kbar at 630°C. The final temperature, pressure, mineral compositions, and whole-rock mineral modes are the same in the two cases. However, the mineral textures are different, allowing the two paths to be distinguished. The critical information that permits the paths to be discriminated is the recognition of textures that show that the higher-pressure rock originally had more garnet and less staurolite than the lower-pressure rock. There also is a difference in the reactions that produced sillimanite: in the isobaric heating case, most sillimanite is produced by staurolite breakdown, whereas in the isothermal decompression case, most sillimanite is produced by garnet breakdown. The different mechanisms of sillimanite formation cause the rock that decompressed to have much less biotite in the matrix than the rock that was heated. The textures produced for each path are distinct, easily recognizable, and should persist over a wide range temperature and pressure, making it possible to identify them even if the rock undergoes multiple prograde or retrograde events. The simulations show that considerable information about the P–T history of metamorphism is recorded in textures produced by mechanisms of reaction in metapelites. Integration of this technique with regional studies of metamorphic textures has the potential to provide significant constraints on the detailed 3-D thermal history of mountain belts and valuable insight into the tectonic processes that produce them.

Keywords: metamorphic textures, reaction mechanisms, P–T–t path, irreversible thermodynamics, differential thermodynamics.

SOMMAIRE

On utilise une technique de modelisation progressive fondée sur les relations thermodynamiques différentielles et irréversibles afin de mieux comprendre les subtilités texturales des roches dans des socles ayant subi un métamorphisme régional. Deux tracés différents d'évolution P–T sont évalués dans la production d'une schiste à sillimanite–grenat à partir d'une schiste à staurolite–grenat de la même composition globale. Le premier tracé implique un réchauffement isobare de 600°C à 630°C à 4 kbar, et le deuxième, une décompression isotherme de 8 à 4 kbar à 630°C. La température, la pression, la composition des minéraux, et les proportions modales des minéraux de la roche sont les mêmes dans les deux cas. En revanche, les textures des minéraux sont différentes, ce qui permet de les distinguer. Pour permettre cette distinction, il est nécessaire de reconnaître, d'après les textures, que la roche équilibrée à pression élevée avait, à l'origine, plus de grenat et moins de staurolite que la roche équilibrée à pression plus faible. Il y a aussi une différence dans les réactions responsables de la formation de la sillimanite: dans le cas d'un réchauffement isobare, la plupart de la sillimanite se forme par déstabilisation de la staurolite, tandis que dans le cas d'une décompression isotherme, la plupart de la sillimanite résulte de la déstabilisation du grenat. A cause des différents mécanismes de formation de la sillimanite, la roche sujette à la décompression possède beaucoup moins de biotite dans la matrice que la roche qui a été réchauffée. Les textures résultant de chaque tracé évolutif sont distinctes, facilement reconnaissables, et devraient persister sur un grand intervalle de température et de pression, de sorte qu'on devrait pouvoir les identifier même si la roche a subi de multiples événements progrades ou rétrogrades. Les simulations montrent qu'une riche information à propos de l'évolution P–T du métamorphisme serait préservée dans les textures produites selon les mécanismes de réaction dans les métapélites. L'intégration de cette technique avec l'étude du développement régional de textures métamorphiques a le potentiel d'ajouter des contraintes importantes sur le développement thermique des ceintures orogéniques en trois dimensions, et sur les processus tectoniques qui en sont responsables.

(Traduit par la Rédaction)

Mots-clés: textures métamorphiques, mécanismes de réaction, tracé P–T–t, thermodynamique irréversible, thermodynamique différentielle.

[1] *E-mail address*: tom-foster@uiowa.edu

Introduction

One of the main goals of metamorphic studies is to obtain detailed information about the sequence of P–T conditions to which rocks have been subjected to during orogeny (the P–T path). These data provide important constraints for thermal and tectonic models of the evolution of a mountain belt because they are closely linked to the thermal and tectonic history of an area. Consequently, methods that lead to better information about P–T path promise to substantially improve knowledge of processes that operate in the deep parts of orogenic belts. Presently, most investigators try to deduce the P–T path of a rock using a combination of field studies, thermobarometry, techniques that predict reactions at the whole-rock scale (such as the Gibbs method) and qualitative interpretation of textures and fabrics. A notable exception is found in the work of Kretz (1966, 1969, 1973, 1974, 1993, 1994), who has pioneered innovative quantitative approaches to metamorphic textures. His work has provided the foundation for a number of recent studies (*e.g.,* Carlson 1989, 1991, Carlson & Denison 1992, Carlson *et al.* 1995, Denison *et al.* 1997a, b) that are providing considerable insight into metamorphic textures and the processes that form them.

Many petrologists recognize that the interpretation of metamorphic textures has the potential to provide considerable insight into the P–T history of a rock, but this approach is presently of limited value because most textural interpretations are based on qualitative assessments that are essentially "guesses" about what a texture represents. Textures hold great promise for the interpretation of P–T paths because many metamorphic reactions proceed by a mechanism that involves non-isochemical reactions in local domains. These reactions produce subtle, but distinct, variations in the modes of common minerals (*e.g.,* biotite, muscovite, plagioclase, quartz) that are stable over a wide range of metamorphic conditions. These variations form compositionally distinct regions that persist through much of the P–T history of a rock, but only the most obvious cases are typically recognized. In this paper, I demonstrate how differential and irreversible thermodynamics can be used to simulate the mechanisms of reaction that form metamorphic textures, and how these mechanisms relate to the P–T history of a rock.

Background

An approach that is widely used to extract P–T paths from textures and zoning profiles was developed by Spear (1988, Spear *et al.* 1991). It uses differential thermodynamics (the Gibbs method) and mass balance (Duhem's Theorem) to calculate whole-rock modal composition, mineral compositions and zoning profiles in porphyroblasts that should be produced by a specified P–T trajectory. Where carefully applied, this technique has provided considerable insight into the evolution of metamorphic rocks in orogenic belts. Spear (1993) and Spear *et al.* (1995) gave examples of the wide range of problems that are being addressed using this technique.

Their approach has a major limitation: it does not provide information about the local mechanisms of reaction that yield the whole-rock reaction. In a rock containing porphyroblasts, this presents a problem, because the proximity of porphyroblasts to one another can have a profound influence on the mechanism of reactions that develop and the resulting textures (Foster 1983, 1986a, 1998). For example, the proximity of staurolite porphyroblasts to depletion mantles that develop around growing segregations of sillimanite determines the type of pseudomorph that replaces the staurolite as it breaks down (Foster 1983). Porphyroblasts close to the site of sillimanite growth will be enveloped by a muscovite-free mantle and replaced by biotite + plagioclase pseudomorphs. Staurolite farther away from the sillimanite lie beyond the mantles and are replaced by muscovite-rich pseudomorphs. Rocks with low modal amounts of muscovite, such as those near File Lake, Manitoba (Bailes & McRitchie 1978, Bailes 1980), have a wide muscovite-free mantle around sillimanite segregations. Consequently, most staurolite porphyroblasts lie within the mantles, and the predominant pseudomorphic assemblage is biotite + plagioclase. Rocks with abundant modal muscovite, such as those from western Maine (Foster 1977), have thin muscovite-free mantles. Most staurolite porphyroblasts in these rocks lie outside the mantles, and the predominant pseudomorph type is muscovite-rich. This process produces two distinctly different pseudomorphs after staurolite, even though the same whole-rock reaction (St + Ms + Qtz $\rightarrow$ Bt + Sil + Grt + H_2O) is responsible for the consumption of staurolite.

These types of processes can be quantitatively modeled using the irreversible thermodynamic approach of Fisher (1975, 1977). The resulting simulations closely reproduce metamorphic textures observed in a wide variety of rocks and provide insight into the controls on the mechanisms of reaction responsible for metamorphic textures. For example, Foster (1977) originally described biotite-rich and muscovite-rich pseudomorphs such as those discussed above, but their relationship to the muscovite-free mantles of sillimanite segregations was not recognized until the model calculations predicted their development. This technique has mostly been applied to textures that developed over short segments of P–T paths (*e.g.,* Foster 1981, 1982, 1983, 1986a, 1990, 1991, Dutrow & Foster 1992, Guidotti *et al.* 1996) because the net amount of porphyroblast growth or dissolution at the whole-rock scale can be determined from field relations and least-squares techniques using minerals of fixed compositions. The Gibbs method as implemented by Spear *et al.* (1991) provides a way to monitor whole-rock reactions, mineral modes

and mineral compositions along an entire P–T path. This information can be integrated with irreversible thermodynamic models of local reactions to provide a detailed simulation of mechanisms of reaction that develop along a specified P–T path (Foster 1992, 1994). To illustrate the power of this method, textures produced by two different P–T paths (Fig. 1) on rocks with the same bulk composition and peak P–T conditions will be calculated and compared.

Textures for Two P–T Paths

The reference rock used in the calculations was derived from the reference rock used by Spear *et al.* (1995) and has a composition similar to metapelites near Rangeley, Maine. The parameters for the reference rock are given in Table 1. The stability fields of phases (Fig. 1) for this bulk composition in a system open to H_2O were calculated using the Gibbs90 program (Spear *et al.* 1991). The P–T paths used in the calculations (Fig. 1) were selected to illustrate how two rocks with the same bulk composition and P–T conditions develop different textures depending upon the P–T path they followed. The two distinct paths are similar to those commonly proposed in metamorphic terranes: an isobaric heating path (rock A) and an isothermal decompression path (rock B).

The examples both start with a staurolite – garnet – biotite – muscovite – plagioclase – quartz schist and terminate with a sillimanite–garnet schist above the staurolite-out isograd at 630°C, 4 kbar (Fig. 1, point C). The starting modes and mineral compositions (Table 1) were calculated from the reference rock by removing chlorite and sillimanite from the assemblage and changing the T and P from the reference conditions to 600°C, 4 kbar (rock A) or 630°C, 8 kbar (rock B) with the system open to H_2O fluid. The bulk composition is the same in both rocks except that rock B has slightly less H_2O, because the higher-pressure assemblage contains more garnet and a lower proportion of hydrous minerals. The final rock (at point C, Fig. 1) in both cases will have nearly identical modal mineralogy and mineral compositions at the same final P–T conditions, so that the major differences between the rocks are the textures created by the local mechanisms of reaction that develop along the P–T path. The rock in the first example (path A) represents an isobaric heating event that is typical of regional metamorphism related to the intrusion of magmas at a mid-crust depth (Spear 1993, p. 66). The rock in the second example (path B) is similar to the decompression portion of a clockwise P–T path, which is characteristic of crustal thickening (Spear 1993, p. 62). Mineral modes and mineral compositions for each path are given in Figure 2.

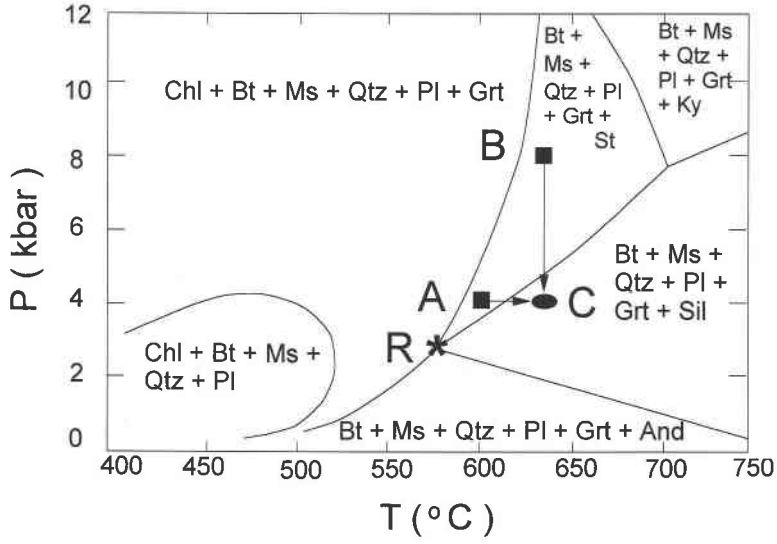

Fig. 1. P – T diagram showing stable mineral assemblages in systems open to H_2O. Diagram was calculated from reference rock given in Table 1 using the Gibbs 90 program (Spear *et al.* 1991) with mass-balance constraints, the program variable NFRAC = 0 for all minerals and NFRAC = 2 for H_2O (no zoning in minerals, system open to H_2O). Point A: starting conditions for path of isobaric heating (rock A). Point B: starting conditions for path of isothermal decompression (rock B). Point C: final conditions for both paths. Point R (*): conditions of reference rock (Table 1). Small fields with K-feldspar and cordierite assemblages in the lower right corner of the diagram are not shown to allow more pertinent regions to be clearly labeled.

The textures for the starting conditions in both rocks were chosen to consist of six staurolite crystals and six garnet crystals set in a foliated matrix of muscovite – biotite – plagioclase and quartz. Because of the modal differences in the two P and T settings, this configuration causes the higher-pressure rock (rock B) to have larger crystals of garnet and smaller crystals of staurolite than the lower-pressure rock (rock A). The matrix of the higher-pressure rock also has noticeably less biotite than the lower-pressure rock. The starting textures for rocks A and B are shown in Figures 3a and 4a, respectively. The mineral modes and compositions are given in Table 1.

The basic procedure to predict the textures in each rock as they progress along their specified P–T paths involves two steps, one to calculate the whole-rock reaction, and the other to calculate the local mechanisms of reaction by which the whole-rock reaction proceeds. The whole-rock reactions are simulated by using the Gibbs 90 program (Spear *et al.* 1991), which calculates the mineral modes and compositions in the rock as it proceeds along the P–T path. The whole-rock reaction and mineral compositions along the P–T path from the Gibbs program are used as input for the program SEG 93 (Foster 1993), which models local reactions that develop in the vicinity of porphyroblasts or mineral segregations. The method assumes that: 1) local equilibrium is maintained along the P–T path, 2) chemical potential gradients driving material transport are sufficiently small that the mineral compositions for each P–T increment are essentially the same throughout a thin section, 3) there is no appreciable flow of fluid through the outcrop, and 4) the rocks are not under a significant deviatoric stress. In addition, the diffusion coefficients for all components were assumed to be identical. These assumptions appear to be well founded for at least some metamorphic rocks because previous modeling studies using them have produced a wide variety textures with morphologies and modes that are very similar to those observed in amphibolite-facies metapelites (Foster 1994, Guidotti *et al.* 1996). Although estimates of relative thermodynamic diffusion coefficients for transport along grain boundaries in low-pressure upper-amphibolite-facies metapelites are available (Foster 1981), this study used coefficients that are equal for all components ($L_{ii} / L_{jj} = 1$) because it is uncertain whether or not the previously determined values are valid over a wide range of P–T conditions. As in Foster (1981), cross terms in the diffusion coefficient matrix were set to zero ($L_{ij} = 0, i \neq j$). Test calculations show that similar local reactions are produced by both sets of coefficients, resulting in similar textures. However, variations in relative coefficients slightly change the stoichiometry of the local reactions, which results in subtle textural differences that should allow a comprehensive set of values to be determined when quantitative data on texture have been obtained over a wide range of pressures and temperatures.

TABLE 1. MINERAL MODES AND COMPOSITIONS FOR REFERENCE ROCK USED TO CALCULATE FIGURE 1 AND FOR ROCKS A AND B

		Reference rock	Rock A	Rock B
T (°C)		571	600	630
P (bars)		2653	4000	8000
Mineral volumes (cm^3)				
Qtz (1)		31.0	29.3	25.7
AlSil (24)		0	–	–
Bt (10)		23.0	17.3	5.7
Ms (6)		23.0	28.2	38.7
St (12)		15.0	11.0	2.6
Pl (8)		5.0	4.3	3.2
Grt (9)		3.0	8.9	20.9
Chl (14)		0	–	–
Mineral compositions				
Biotite	X_{phl}	0.285	0.336	0.494
	X_{ann}	0.713	0.663	0.506
	X_{MnBt}	0.002	0.001	0.0004
Garnet	X_{prp}	0.060	0.082	0.151
	X_{alm}	0.840	0.848	0.801
	X_{sps}	0.050	0.021	0.009
	X_{grs}	0.050	0.048	0.038
Staurolite	X_{MgSt}	0.088	0.114	0.198
	X_{FeSt}	0.905	0.884	0.801
	X_{MnSt}	0.007	0.003	0.001
Plagioclase	X_{ab}	0.602	0.705	0.918
	X_{an}	0.398	0.295	0.082
Chlorite	X_{MgChl}	0.309	–	–
	X_{FeChl}	0.690	–	–
	X_{MnChl}	0.001	–	–

Number in parentheses after mineral abbreviation is phase number in Gibbs90 data file used in calculations. A dash means that the phase is not present in the rock, a zero means the phase is present in an infinitesimally small amount. Mineral abbreviations according to Kretz (1983).

P–T path A: isobaric heating

Initially, rock A is a staurolite–garnet schist with a foliated matrix consisting of biotite, muscovite, plagioclase and quartz at 600°C, 4 kbar. Mineral modes and mineral compositions for this rock are given in Table 1. Heating rock A at 4 kbar (Fig. 1) produces very little reaction until staurolite begins to break down to sillimanite at 608°C (Fig. 2a). The reaction mechanism that develops is strongly influenced by the pattern of sillimanite nucleation (Foster 1986b). Because the factors controlling the patterns of nucleation are poorly understood, two end-member cases are considered here: one with few nuclei and one with many nuclei. Although a number of factors influence the development of nuclei, these two end-member cases are taken to indicate different rates of overstepping of a reaction. Few nuclei are favored where reaction rates and transport rates between reaction sites are able to keep pace with heating, whereas many nuclei are considered to represent situations where the reaction is rapidly overstepped because

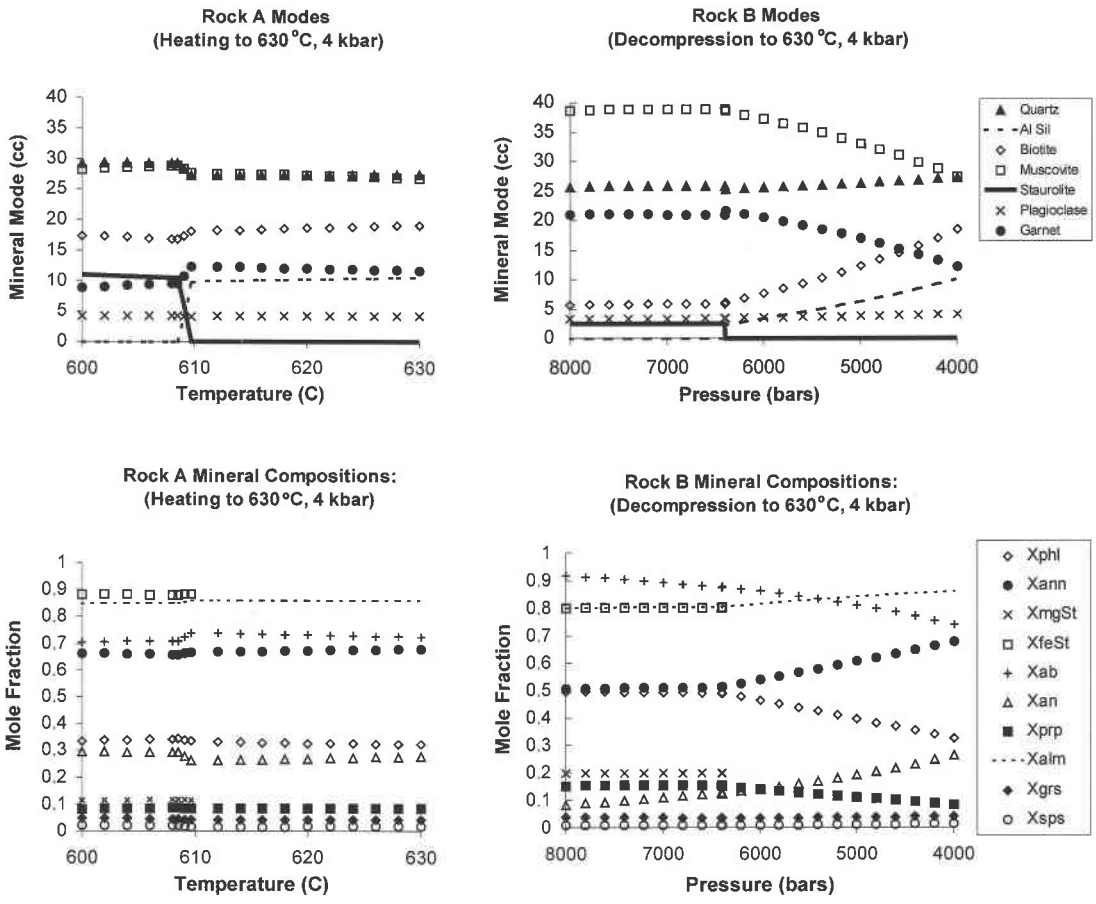

FIG. 2. Mineral modes and compositions for rock A as it progresses from A to C (Fig. 1) along a path of isobaric heating, and for rock B as it progresses from B to C (Fig. 1) along a path of isothermal decompression. Note that final modes and compositions at 630°C, 4 kbar (point C, Fig. 1) are virtually identical in both rocks. The number of oxygen atoms per anhydrous formula unit used in reactions discussed in text is as follows: Ms 22, Bt 22, Qtz 2, Pl 8, Grt 12, St 46, and Sil 5.

reaction rates and transport rates are unable to keep pace with heating (Ridley 1985, Kretz 1994).

In the case of few nuclei, six sillimanite nuclei were allowed to form in the matrix and to begin growing. The constraints on material transport through the matrix around the growing sillimanite result in the reaction:

$$0.25\ \text{Ms} + 0.31\ \text{Pl} \rightarrow 0.03\ \text{Bt} + 1.18\ \text{Qtz} + 1.0\ \text{Sil} \quad (1)$$

(see Appendix for calculation procedure, Fig. 2 for mineral compositions). The components needed to balance this reaction are provided by diffusion of material through the network of grain boundaries in the matrix around the growing sillimanite. Reaction (1) is the sum of several local reactions that consume muscovite and plagioclase in the vicinity of the growing sillimanite and that produce biotite-rich mantles and quartz-rich mantles around the sillimanite (Fig. 3b). Details of the local mechanisms of reaction that allow reaction (1) to proceed are described in Foster (1981, 1982), and good examples of this texture are provided by photomicrographs in Foster (1977, 1982), Bailes & McRitchie (1978), and Bailes (1980).

While sillimanite is growing in one area of the rock, staurolite in other domains of the rock begins to dissolve *via* the local reaction:

$$1.0\ \text{St} + 15.4\ \text{Qtz} \rightarrow 0.44\ \text{Bt} + 1.92\ \text{Ms} + 3.22\ \text{Pl} \quad (2)$$

The constituents needed to balance this reaction are

provided by diffusion of material along the network of grain boundaries in the matrix around the dissolving staurolite. Because the quartz must come from the matrix around the porphyroblast and the staurolite must come from the porphyroblast, reaction (2) splits into two parts, one that consumes the porphyroblast (3) and the other that progresses out into the matrix (4).

$$1.0\ \text{St} \rightarrow 2.01\ \text{Ms} \quad (3)$$

$$15.4\ \text{Qtz} + 0.09\ \text{Ms} \rightarrow 0.44\ \text{Bt} + 3.22\ \text{Pl} \quad (4)$$

This split results in the replacement of staurolite by a muscovite-rich pseudomorph and the reaction of matrix quartz to form a mantle enriched in biotite + plagioclase that grows into the matrix around the pseudomorph (Fig. 3b). If the staurolite was a poikiloblast with quartz inclusions, it would have been replaced by a muscovite-rich pseudomorph containing biotite as well as plagioclase, because the quartz needed for reaction (2) would be supplied from the inclusions, rather than a reaction that consumed matrix quartz (Foster 1981, 1983). Photomicrographs of this texture are available in Foster (1977, 1983).

The growth of sillimanite is linked to the dissolution of staurolite by the components diffusing along the network of grain boundaries in the matrix around each segregation so that the local reactions form a reaction cycle that produces the whole-rock reaction (Carmichael 1969). Reaction (1) produces ~9.8% (volume percent of rock) sillimanite, and reaction (2) consumes ~11% staurolite in rock A. In addition, a small amount (~1.6%) of garnet growth is required to balance the whole-rock reaction (Fig. 2a). The local reaction needed to grow garnet that is consistent with material-transport constraints in the matrix around the garnet is:

$$0.48\ \text{Bt} + 0.68\ \text{Pl} \rightarrow 0.02\ \text{Ms} + 1.62\ \text{Qtz} + 1.0\ \text{Grt} \quad (5)$$

The constituents needed to balance reaction (5) are provided or removed by diffusion through the grain-boundary matrix around the garnet and are transported through the matrix to the sillimanite or staurolite, where they balance reactions (1) or (2), respectively. Reaction (5) produces a biotite-poor region around garnet as it grows (Fig. 3b), but the mantle is relatively thin because of the small amount of garnet growth and the large size of the pre-existing porphyroblasts of garnet. In a rock with a coarser matrix than shown in Figure 3b, the mantle will be diffuse and difficult to detect because the matrix would not be homogeneous at the scale of the mantle thickness. Reactions (1), (2) and (5) take place simultaneously in the rock, allowing the overall whole-rock reaction to proceed in a reaction cycle of the type proposed by Carmichael (1969). The matrix minerals, especially the micas, act as catalysts to facilitate the whole-rock reaction (Foster 1991). The sources and sinks in the different local reactions balance each other, and the rock is closed at the whole-rock scale to all components except H_2O, which is allowed to escape. When the staurolite-breakdown reaction is complete, the rock contains 9.8% sillimanite, 12.8% garnet and 0% staurolite. An example of a rock with this type of texture is shown in Foster (1977, Fig. 5).

Once the staurolite is totally consumed, the amount of sillimanite growth per degree of temperature rise drastically decreases. Figure 3b shows the rock at 610°C, 4 kbar, just after staurolite has been consumed. Further heating to 630°C produces a small amount (0.7%) of sillimanite and biotite growth at the expense of garnet and muscovite (Fig. 2a). This addition causes the sillimanite segregation to continue to grow slightly *via* a reaction similar to (1). Simultaneously, garnet dissolves slightly (–0.8%) because of a reaction that is the reverse of (5), causing garnet to be rimmed by a thin layer of biotite plus a small amount of plagioclase. No reaction takes place at the staurolite pseudomorph during this temperature interval because the phases making up the pseudomorph are the same as in the stable matrix that surrounds it. The textures in the rock at 630°C, 4 kbar are shown in Figure 3c. Note that several compositionally distinct regions are shown in this figure: areas rich in sillimanite, areas rich in muscovite, areas rich in garnet, and the matrix. These areas now have a different bulk-composition than the matrix from which they formed. The local compositional difference will have a strong influence on future textures that develop in the rock. Evidence of these local compositional variations will persist over a wide range of temperatures and pressures, allowing the configuration shown in Figure 3c to be identified even after additional reactions have taken place in the rock.

If sillimanite nucleates at many sites instead of few sites, the same whole-rock reaction leading to sillimanite and garnet at the expense of staurolite will take place (Fig. 2a), but by a different mechanism. The presence of sillimanite nuclei and quartz in the matrix surrounding the staurolite causes the local staurolite-consuming reaction to proceed *via*:

$$1.0\ \text{St} + 3.0\ \text{Qtz} + 0.75\ \text{Ms} \rightarrow 0.75\ \text{Bt} + 10.5\ \text{Sil} \quad (6)$$

Reaction (6) differs from reaction (2) owing to the constraint on transport of Si and Al through the matrix provided by the Gibbs–Duhem equations of sillimanite and quartz, which requires that the chemical potential gradients of $AlO_{1.5}$ and SiO_2 be zero. This forces reaction (6) to conserve Al and Si, resulting in the production of large amounts of sillimanite. As in the case of reaction (2), reaction (6) splits into two parts. The staurolite for reaction (6) is supplied *via* a reaction that replaces the staurolite porphyroblast:

$$1.0\ \text{St} \rightarrow 0.21\ \text{Bt} + 8.29\ \text{Sil} \quad (7)$$

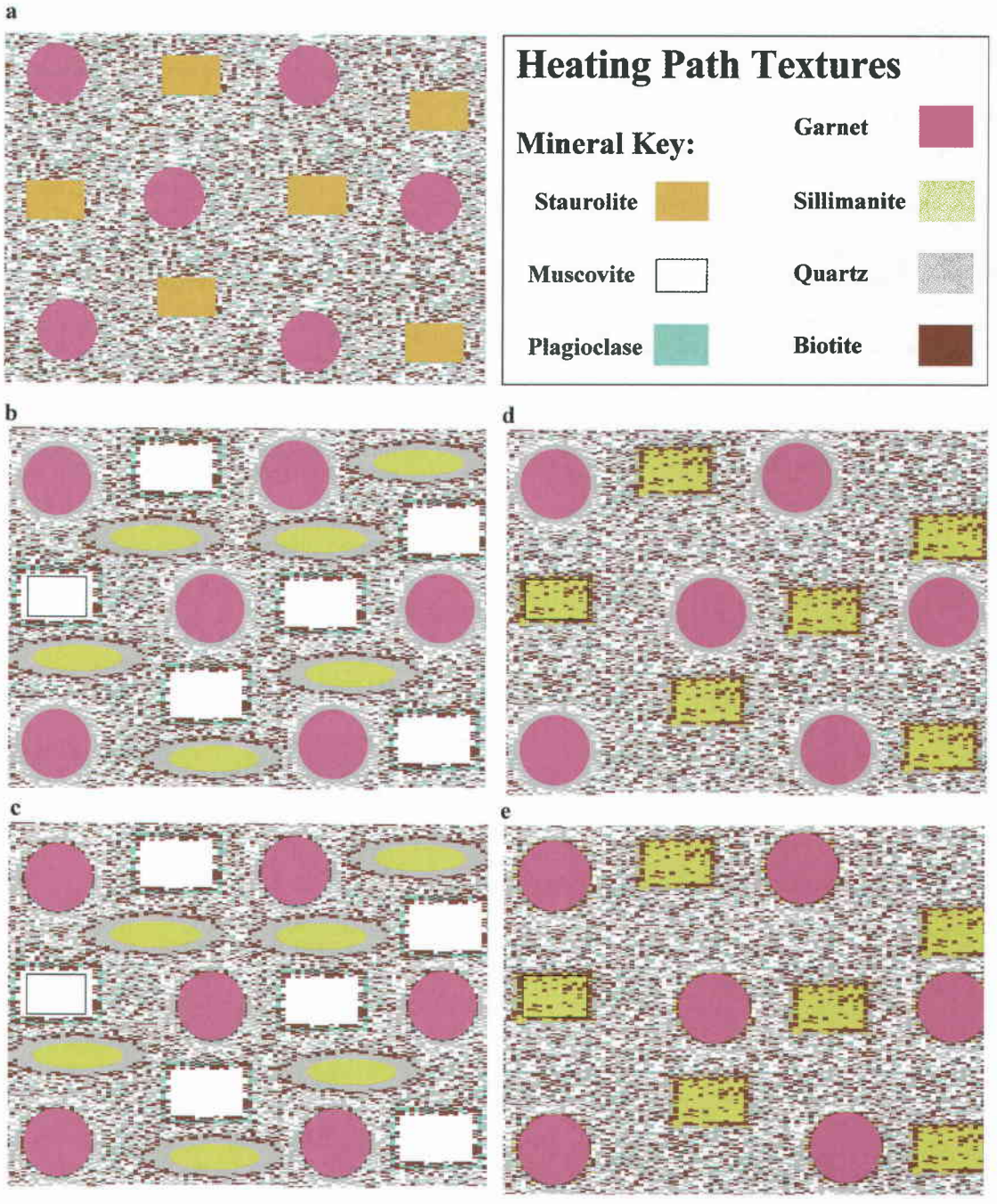

FIG. 3. Calculated textures for path of isobaric heating (rock A). Horizontal length of each frame is 2 cm. Minerals are color-coded according to key in upper right corner. a) Starting texture for rock A (600°C, 4 kbar). b) Textures after staurolite breakdown is complete where few nuclei of sillimanite form (610°C, 4 kbar). Black rectangle in center left pseudomorph shows original position of staurolite porphyroblast. c) Textures at end of path of isobaric heating where few nuclei of sillimanite form (630°C, 4 kbar). d) Textures after staurolite breakdown is complete where many nuclei of sillimanite form (610°C, 4 kbar). e) Textures at end of path of isobaric heating where many nuclei of sillimanite form (630°C, 4 kbar).

and the quartz and muscovite are supplied by a reaction that progresses out into the matrix around the porphyroblast:

$$3.0\ Qtz + 0.75\ Ms \rightarrow 0.54\ Bt + 2.21\ Sil \quad (8)$$

The result of reactions (7) and (8) is that the staurolite is replaced by a sillimanite-rich pseudomorph (Sil > Bt); it is surrounded by a biotite-rich mantle (Bt > Sil) that replaced quartz and muscovite in the matrix around the porphyroblast. As in the case described for few nuclei of sillimanite, a small amount of garnet growth is required to balance the constituents produced or consumed by reaction (6). The garnet is produced by reaction (5), which results in a biotite-poor mantle around the garnet that is exactly the same as the mantle around the garnet in the situation of few nuclei of sillimanite. The texture for many nuclei of sillimanite at 610°C, after all of the staurolite has been consumed, is shown in Figure 3d.

Further heating will cause garnet to begin to dissolve *via* the reaction:

$$1.0\ Grt + 0.54\ Ms \rightarrow 0.54\ Bt + 0.80\ Qtz + 0.05\ Pl + 2.05\ Sil \quad (9)$$

which replaces the garnet with a biotite + sillimanite intergrowth. Because the muscovite for reaction (9) must come from the matrix and the garnet must come from the porphyroblast, reaction (9) splits into two parts. One replaces garnet:

$$1.0\ Grt \rightarrow 0.43\ Bt + 0.54\ Sil \quad (10)$$

and another consumes muscovite in the matrix:

$$0.54\ Ms \rightarrow 0.11\ Bt + 0.80\ Qtz + 0.05\ Pl + 1.51\ Sil \quad (11)$$

Reaction (10) replaces the garnet with a thin layer that is biotite-rich but contains smaller amounts of sillimanite. Reaction (11) replaces matrix muscovite near the garnet with a thin sillimanite-rich mantle that also contains biotite, quartz and plagioclase (Fig. 3e). The pseudomorphs of sillimanite after staurolite do not take part in this reaction because they are isolated from the garnet by the material-transport constraints in the matrix that force the chemical potential gradients of $AlO_{1.5}$ and SiO_2 to be fixed at zero in the matrix. This effectively isolates the sillimanite that grew from the staurolite from that which grew from the garnet. Again, the textures have produced local changes in composition that will strongly influence the development of further mechanisms of reaction, allowing evidence of the texture shown in Figure 3e to persist over a wide range of T and P.

P–T path B: isothermal decompression

The beginning texture for rock B is a schist with six porphyroblasts of staurolite and six porphyroblasts of garnet set in a foliated matrix consisting of biotite, muscovite, plagioclase and quartz at 630°C, 8 kbar. Note that rock B has larger crystals of garnet and smaller crystals of staurolite than rock A and less biotite in the matrix (Fig. 4a). Lowering pressure in this rock at 630°C (Fig. 1) produces a reaction that, provided the rock is open to H_2O, should produce staurolite at the expense of garnet until the sillimanite field is reached at about 4.8 kbar. However, this reaction consumes H_2O, which needs to be supplied to the rock for the reaction to proceed, a situation that is rare in typical prograde regional metamorphic settings. If H_2O is not allowed to infiltrate the rock during decompression, the available H_2O along grain boundaries is quickly consumed by the formation of a small amount of staurolite. Then the rock no longer is H_2O-saturated, and the H_2O content of the rock will remain constant, with dry grain-boundaries as the pressure decreases. Under these conditions, little reaction occurs until the sillimanite-forming curve is crossed at 6.4 kbar. This curve is displaced ~1.6 kbar higher than the curve shown on Figure 1 because the lower content of H_2O in rock B decreases the stability field of staurolite. When sillimanite begins to form, H_2O is produced, saturates the grain boundaries, and excess H_2O will escape from the rock. As in the case of isobaric heating, the reaction mechanism that develops is strongly influenced by the pattern of sillimanite nucleation (Foster 1986b). Again, two end-member cases are considered here: one with few nuclei and one with many nuclei.

If few sillimanite nuclei form in the matrix, the sillimanite-producing reaction is similar to reaction (1), but the stoichiometry is slightly different because of the compositional variation in the minerals due to different P and T:

$$0.27\ Ms + 0.23\ Pl \rightarrow 0.04\ Bt + 1.10\ Qtz + 1.0\ Sil \quad (12)$$

The sillimanite segregations produced by this reaction (Fig. 4b) have a similar morphology to the ones (Fig. 3b) produced by reaction (1), but the size of the segregations is smaller because of the lower amount of staurolite, which is completely consumed after only 2.3% sillimanite grows in the rock.

The staurolite in rock B is replaced by a reaction similar to reaction 2, but with slightly different stoichiometry:

$$1.0\ St + 14.2\ Qtz \rightarrow 0.31\ Bt + 2.18\ Ms + 2.35\ Pl \quad (13)$$

The size of the pseudomorphs produced by reaction (13) is smaller than those produced by reaction (2) owing to the smaller size of the staurolite crystals originally present in rock B. Reaction (13) splits into two reactions: one that replaces staurolite, which is similar to reaction (3), and one that consumes quartz in the matrix around the porphyroblast, which is similar to reaction (4). As in the case of isobaric heating, a small

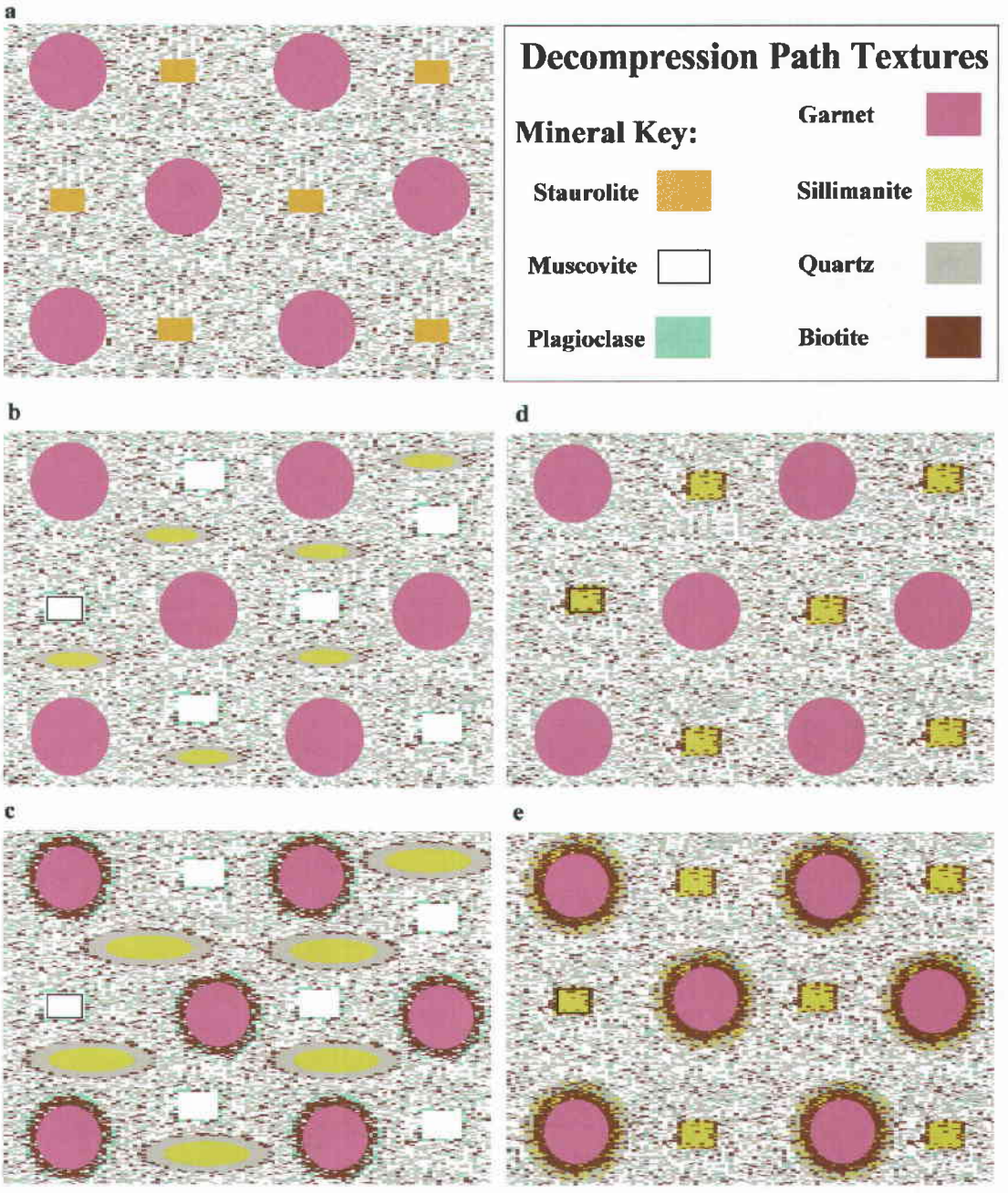

FIG. 4. Calculated textures for path of isothermal decompression (rock B). Horizontal length of each frame is 2 cm. Minerals are color-coded according to key in upper right corner. a) Starting texture for rock B (630°C, 8 kbar). b) Textures after staurolite breakdown is complete where few nuclei of sillimanite form (630°C, 6.4 kbar). Black rectangle in center left pseudomorph shows original position of staurolite porphyroblast. c) Textures at end of path of isothermal decompression where few nuclei of sillimanite form (630°C, 4 kbar). d) Textures after staurolite breakdown is complete where many nuclei of sillimanite form (630°C, 6.4 kbar). e) Textures at end of isothermal decompression path where many nuclei of sillimanite form (630°C, 4 kbar).

amount of garnet growth is required to balance the local reactions that cause the breakdown of staurolite and growth of sillimanite. Such growth proceeds *via* a reaction similar to (5):

$$0.41\ \text{Bt} + 0.47\ \text{Pl} + 0.05\ \text{Ms} \rightarrow 1.0\ \text{Grt} + 1.17\ \text{Qtz} \quad (14)$$

The rock with few nuclei of sillimanite after staurolite has been consumed is shown in Figure 4b. It is similar to the rock in the case of isothermal heating (rock A) after staurolite breakdown except that the sillimanite segregations and staurolite pseudomorphs are smaller, and the garnet crystals are larger in the decompression case (rock B).

Upon further decrease in pressure, garnet breaks down to sillimanite in the whole-rock reaction (Fig. 2). If no new nuclei of sillimanite form, the sillimanite-forming reaction continues to be reaction (12), and garnet is replaced by a reaction that is the reverse of (14), with small differences in stoichiometry because of compositional changes in minerals along the reaction path:

$$1.0\ \text{Grt} + 1.44\ \text{Qtz} \rightarrow 0.46\ \text{Bt} + 0.02\ \text{Ms} + 0.56\ \text{Pl} \quad (15)$$

This reaction splits into two parts, one that replaces the garnet with biotite and lesser amounts of muscovite and plagioclase (16), and the other that provides the quartz for reaction (15) by converting matrix quartz and some muscovite to biotite and plagioclase (17).

$$1.0\ \text{Grt} \rightarrow 0.41\ \text{Bt} + 0.09\ \text{Ms} + 0.08\ \text{Pl} \quad (16)$$

$$0.07\ \text{Ms} + 1.44\ \text{Qtz} \rightarrow 0.48\ \text{Pl} + 0.05\ \text{Bt} \quad (17)$$

This produces a plagioclase-rich mantle around the garnet and a biotite-rich pseudomorph after the garnet. The rock at the end of the decompression-induced reaction path with few nuclei of sillimanite is shown in Figure 4c. It is characterized by muscovite pseudomorphs after staurolite, sillimanite segregations with a biotite-rich rim, and biotite-rich pseudomorphs after garnet with an outer mantle that is plagioclase-rich.

If sillimanite nucleates at many sites throughout the rock when staurolite begins breaking down at 6.4 kbar, the staurolite will dissolve in a matrix that contains abundant nuclei of sillimanite. The constraints on material transport through the matrix provided by the Gibbs–Duhem relations of sillimanite and the other matrix minerals result in the production of a sillimanite-rich pseudomorph after staurolite *via* the reaction:

$$1.0\ \text{St} + 0.67\ \text{Ms} + 2.85\ \text{Qtz} \rightarrow 10.36\ \text{Sil} + 0.67\ \text{Bt} \quad (18)$$

This reaction splits into two parts, one consuming staurolite (19) and the other consuming muscovite and quartz in the matrix (20):

$$1.0\ \text{St} \rightarrow 0.15\ \text{Bt} + 8.41\ \text{Sil} \quad (19)$$

$$0.67\ \text{Ms} + 2.85\ \text{Qtz} \rightarrow 0.52\ \text{Bt} + 1.95\ \text{Sil} \quad (20)$$

This produces a sillimanite-rich pseudomorph after staurolite, which is surrounded by a biotite-rich rim, as shown in Figure 4d. The boundary between the change in mode at the pseudomorph–mantle boundary is the original location of the matrix–staurolite boundary. A small amount of garnet growth (0.7%) is required to balance the whole-rock staurolite-breakdown reaction (Fig. 2b). Sillimanite nuclei in the matrix around the garnet are quickly consumed by garnet growth *via* a reaction that is similar to the reverse of reaction (9). Then the growth of garnet proceeds *via* reaction (14). This reaction slightly increases the size of the garnet porphyroblasts and consumes nearby biotite and plagioclase. The rock, after all the staurolite has broken down at 6.4 kbar, is shown in Figure 4d. It is characterized by small pseudomorphs of sillimanite after staurolite with a biotite-rich rim, and large crystals of garnet with subtle biotite-depleted zones around them.

Upon further decompression, garnet shifts to the reactant side of whole-rock reaction as more sillimanite forms (Fig. 2b). Sillimanite nuclei forming in the matrix near the garnet should not be consumed, but instead would be expected to grow owing to the local reaction near the garnet:

$$1.0\ \text{Grt} + 0.53\ \text{Ms} \rightarrow 0.53\ \text{Bt} + 0.03\ \text{Pl} + 0.88\ \text{Qtz} + 2.04\ \text{Sil} \quad (21)$$

This reaction splits into two parts, one consuming garnet (22) and the other consuming muscovite from the matrix (23):

$$1.0\ \text{Grt} \rightarrow 0.42\ \text{Bt} + 0.56\ \text{Sil} \quad (22)$$

$$0.53\ \text{Ms} \rightarrow 0.11\ \text{Bt} + 0.03\ \text{Pl} + 0.88\ \text{Qtz} + 1.48\ \text{Sil} \quad (23)$$

The garnet is replaced by a biotite + sillimanite pseudomorph that is biotite-rich, and the matrix is replaced by a biotite + sillimanite mantle around the pseudomorph that is sillimanite-rich. Note that most (~75%) of the sillimanite production is actually in the mantle around the garnet rather than in the garnet pseudomorph. Garnet-replacement textures with similar features in rocks from Connemara, Ireland, are illustrated in Yardley (1977, Fig. 1C). The production of a large amount of sillimanite in the muscovite-consuming reaction arises because this is one of the few situations where Al is truly immobile in metamorphic rocks. The presence of sillimanite nuclei plus quartz in local equilibrium throughout the matrix forces the chemical potential gradient of $AlO_{1.5}$ to be zero, requiring that all

reactions conserve aluminum. The large amount of muscovite required to satisfy reaction (21) releases abundant Al, which is consumed by formation of sillimanite in reaction (23). Some of the potassium released by the muscovite breakdown in (23) is consumed locally by biotite production in reaction (23), and the rest diffuses across the biotite + sillimanite pseudomorph to the remaining garnet, where it is used to make biotite at the expense of garnet in reaction (22). The sillimanite that formed in the pseudomorphs after staurolite (at 6.4 kbar) does not grow as the pressure decreases because of the inability of aluminum to be transported through the matrix from the site of garnet reaction to the location of the sillimanite-rich staurolite pseudomorphs. The rock at 630°C, 4 kbar, after the decompression path is complete, is shown in Figure 4e. It has large crystals of garnet rimmed by sillimanite + biotite and small sillimanite-rich pseudomorphs after staurolite, with biotite concentrated at the rim.

Discussion and Conclusions

The modal composition of a rock is very sensitive to P and T, as are mineral compositions (Fig. 2). Consequently, careful analysis of modal variations can yield valuable information about the P–T path of metamorphism. Methods involving modal mineralogy may actually prove to be superior to conventional thermobarometry, which uses mineral compositions, because the modes are more easily recognized and are less likely to be affected by re-equilibration. For example, the starting configurations for rocks A and B were derived from the same bulk composition but have distinctly different initial modes (Figs. 3a, 4a). The distinctions are easily recognized, even in hand specimen.

A record of the mineral modes along a P–T path is preserved in the textures that form as a rock is progressively metamorphosed. The types of textures that develop are strongly dependent upon the local mechanisms of reaction by which the whole-rock reaction progresses. Provided local equilibrium is maintained, the main constraints on the mechanism of the local reaction are the distributions of minerals in the rock, the nucleation sites for new minerals that form, and the constraints on material transport provided by the mineral assemblages in the regions around reaction sites. Variations in mineral compositions with P and T and the relative magnitude of diffusion coefficients also influence the local reactions. However, these generally produce second-order effects that result in subtle changes rather than major differences in texture. The reaction mechanisms produce distinct textures that are strongly dependent on the P–T–t path, which can be interpreted using models calculated using differential and irreversible thermodynamic techniques, as described above. For example, the final rocks (point C, Fig. 1) have essentially the same bulk composition, with the same mineral modes and compositions (Fig. 2) for both cases, isobaric heating (rock A) and isothermal decompression (rock B). However, the textures are distinct (Figs. 3c, e, 4c, e), and their features are easily recognized (Table 2). The crucial information in distinguishing the starting points for the two paths is recognition that rock B came from an environment with more garnet and less staurolite than rock A, indicating that rock B was at a higher pressure than rock A. The evidence that rock A underwent isothermal heating is that most of the sillimanite production is from staurolite breakdown, and only minor amounts come from garnet consumption at the whole-rock scale. Conversely, it can be deduced that rock B followed a path that involved substantial decompression because much of the sillimanite production involved consumption of garnet at the whole-rock scale. The different mechanisms of reaction for the formation of sillimanite also result in different distributions of biotite in the two rocks (Figs. 3c *versus* 4c, Figs. 3e *versus* 4e). Rock A (heating path) has significantly more biotite in the matrix than rock B (decompression path) because much of the biotite in rock B is concentrated around garnet owing to reactions (15) or (21).

As shown in Figures 3 and 4, nucleation patterns play an important role in establishing mechanisms of reaction and the textures that result from them. Although

TABLE 2. COMPARISON OF FEATURES IN ROCKS A AND B

	Rock A isobaric heating	Rock B isothermal decompression
Whole rock		
Final modal proportions	same in both rocks	same in both rocks
Final mineral compositions	same in both rocks	same in both rocks
Sillimanite production	most from breakdown of Staurolite in the whole-rock reaction	most from breakdown of Garnet in the whole-rock reaction
Final textures		
Staurolite pseudomorphs	large or more abundant	small or less abundant
Matrix biotite mode	high	low
Biotite rims on garnet	thin	thick
Plagioclase concentrations near garnet	slight	prominent
Muscovite-free mantle around sillimanite	slightly more biotite; slightly thicker width	slightly less biotite; slightly thinner width
Changes in mode along P–T path		
Sillimanite mode	large increase	large increase
Staurolite mode	large decrease	moderate decrease
Garnet mode	small increase	large decrease
Biotite mode	small increase	large increase
Muscovite mode	small decrease	large decrease
Plagioclase mode	nearly constant	nearly constant
Quartz mode	small decrease	small increase
Changes in mineral composition along P–T path		
Garnet composition	tiny increase in Fe/Mg	moderate increase in Fe/Mg
Plagioclase composition	slight decrease in Ca	large increase in Ca
Biotite composition	small increase in Fe/Mg	large increase in Fe/Mg

the factors that influence patterns of nucleation are not well understood, calculations using *a priori* distributions of nuclei allow the resulting textures to be simulated, permitting whole-rock reactions to be extracted from textures that are similar to those in the model calculations. The number of nuclei is dependent on a number of complex feedback loops involving rates of overstepping due to P–T changes and rates of transport in the rock. These factors influence the size of domains in which nucleation is suppressed by nearby reactions (Carlson 1989, 1991). In addition to determining rates of overstepping, the P–T path may exert a profound influence on patterns of nucleation by controlling whether grain boundaries remain wet or dry as metamorphism progresses. P–T paths dominated by heating tend to involve reactions that continually produce small amounts of H_2O, which wets the grain boundaries as it migrates out of the system. On the other hand, decompression paths in staurolite–garnet rocks produce whole-rock reactions that *consume* H_2O, which would be expected to dry out grain boundaries shortly after decompression begins. This arrests the whole-rock reaction, because of the absence of additional H_2O required for it to progress, and greatly decreases rates of transport in the rock. The lower rates of transport cause the size of regions where nucleation is suppressed around a growing crystal to become extremely small, which favors formation of many nuclei. Consequently, many nuclei are more likely to form in a decompression path. For example, many nuclei of sillimanite would be expected to form in rock B because sillimanite is nucleating in a rock with dry grain-boundaries. Fewer nuclei would be expected to form for the same rate of overstepping in rock A because sillimanite is nucleating in a rock with wet grain-boundaries. In general, isobaric heating should tend to produce textures characterized by few nuclei (Fig. 3c), whereas isothermal decompression should produce textures characterized by many nuclei (Fig. 4e).

The textures produced by mechanisms of reaction that develop during metamorphism are generally long-lived features in a rock because they reflect local changes in bulk composition and commonly are made of minerals with large fields of stability, such as micas, quartz and plagioclase. For example, if the rocks shown in Figures 3c, 3e, 4c and 4e were rehydrated in a later greenschist-facies event, the mica pseudomorphs after staurolite in Figures 3c and 4c should persist because they are composed of minerals (muscovite, biotite, and plagioclase) that are stable in the greenschist facies. The sillimanite in the rocks would be replaced by muscovite in a greenschist-facies rehydration, but the new lower-temperature muscovite would be concentrated in the areas where sillimanite was abundant in the higher-grade rocks. The other features associated with the sillimanite segregation, such as quartz-rich and biotite-rich mantles, would be largely unaffected by the rehydration event, and would retain their spatial relationship to the muscovite that replaced the sillimanite, allowing the features to be recognized.

Deformation can also have an important effect on the mineral textures in a rock and complicates the interpretation of polymetamorphic features. However, textural features composed of minerals present in the matrix of the rock (*e.g.,* the mica pseudomorphs after staurolite in Figs. 3 and 4) should deform, but remain recognizable as compositionally distinct domains even though they have changed their shape. It is also possible to incorporate a VdP term in the Gibbs–Duhem relations used to constrain transport relationships around reaction sites, allowing the effects of a deviatoric stress on local reactions to be assessed. Preliminary work suggests that this approach may be a viable one with which to simulate segregations and porphyroblasts that develop in deforming rocks.

The forward modeling technique outlined here has the potential to provide considerable insight into the evolution of metamorphic textures as a rock migrates along a P–T–t path during metamorphism. Although a number of details involving the significance of nucleation patterns, the controls on mechanisms of reaction in deforming rocks, and the values of diffusion coefficients remain to be established, the features of many metamorphic rocks are effectively simulated by this approach. The technique has been extended to investigate controls on the spatial distribution of textures at the scale of a mountain belt by integrating the texture modeling with three-dimensional thermal models of metamorphic terranes (Foster *et al.* 1996, Dutrow *et al.* 1997). Once it is fully implemented, this method should provide important information about orogenic processes by linking the spatial distribution of mineral textures in a mountain belt to tectonic controls of its thermal structure.

Acknowledgements

This paper is dedicated to Ralph Kretz, who pioneered innovative approaches relating textures in natural samples to the kinetic processes that formed them. Frank Spear, Mike Williams and Robert Martin are thanked for extensive thoughtful comments in reviews that substantially improved the manuscript. The research presented here was supported by N.S.F. grant EAR 9220195 to C.T. Foster.

References

Bailes, A.H. (1980): Geology of the File Lake area. *Manitoba Department of Energy and Mines, Geol. Rep.* **78-1**.

_____ & McRitchie, W.D. (1978): The transition from low to high-grade conditions of metamorphism in the Kisseynew sedimentary gneiss belt, Manitoba. *In* Metamorphism in the Canadian Shield (J.A. Fraser & W.W. Heywood, eds.). *Geol. Surv. Can., Pap.* **78-10**, 155-177.

CARLSON, W.D. (1989): The significance of intergranular diffusion to the mechanisms and kinetics of porphyroblast crystallization. *Contrib. Mineral. Petrol.* **103**, 1-24.

_____ (1991): Competitive diffusion-controlled growth of porphyroblasts. *Mineral. Mag.* **55**, 317-330.

_____ & DENISON, C. (1992): Mechanisms of porphyroblast crystallization: results from high resolution computed X-ray tomography. *Science* **257**, 1236-1239.

_____, _____ & KETCHAM, R.A. (1995): Controls on the nucleation and growth of porphyroblasts: kinetics from natural textures and numerical models. *Geol. J.* **30**, 207-225.

CARMICHAEL, D. M. (1969): On the mechanism of prograde metamorphic reactions in quartz-bearing pelitic rocks. *Contrib. Mineral. Petrol.* **20**, 244-267.

DENISON, C., CARLSON, W.D. & KETCHAM, R.A. (1997a): Three-dimensional quantitative textural analysis of metamorphic rocks using high-resolution computed X-ray tomography. I. Methods and techniques. *J. Metamorphic Geol.* **15**, 29-44.

_____, _____ & _____ (1997b): Three-dimensional quantitative textural analysis of metamorphic rocks using high-resolution computed X-ray tomography. II. Application to natural samples. *J. Metamorphic Geol.* **15**, 45-57.

DUTROW, B.L. & FOSTER, C.T. (1992): Constraints on metamorphic fluid from irreversible thermodynamic modeling of tourmaline-rich pseudomorph formation. *Geol. Soc. Am., Abstr. Program* **24**, A218.

_____, _____, TRAVIS, B. & GABLE, C. (1997): Using thermal modeling and forward models of metamorphic textures to decipher P–T–t–X conditions of regional contact metamorphic terranes. *Trans. Am. Geophys. Union, Eos* **78**, F783 (abstr.).

FISHER, G.W. (1975): The thermodynamics of diffusion controlled metamorphic processes. *In* Mass Transport Phenomena in Ceramics (A.R. Cooper & A.H. Heuer, eds.). Plenum Press, New York, N.Y. (111-122).

_____ (1977): Nonequilibrium thermodynamics in metamorphism. *In* Thermodynamics in Geology (D.G. Fraser, ed.). Reidel, Dordrecht, The Netherlands (381-403).

FOSTER, C.T., JR. (1977): Mass transfer in sillimanite-bearing pelitic schists near Rangeley, Maine. *Am. Mineral.* **62**, 727-746.

_____ (1981): A thermodynamic model of mineral segregations in the lower sillimanite zone near Rangeley, Maine. *Am. Mineral.* **66**, 260-277.

_____ (1982): Textural variations of sillimanite segregations. *Can. Mineral.* **20**, 379-392.

_____ (1983): Thermodynamic models of biotite pseudomorphs after staurolite. *Am. Mineral.* **68**, 389-397.

_____ (1986a): Thermodynamic models of reactions involving garnet in a sillimanite/staurolite schist. *Mineral. Mag.* **50**, 427-439.

_____ (1986b): Some effects of nucleation on development of metamorphic textures. *Geol. Soc. Am., Abstr. Programs* **18**, 605.

_____ (1990): Control of material transport and reaction mechanisms by metastable mineral assemblages: an example involving kyanite, sillimanite, muscovite and quartz. *In* Fluid–Mineral Interactions (R.J. Spencer & I-Ming Chou, eds.). *The Geochemical Society, Spec. Publ.* **2**, 121-132.

_____ (1991): The role of biotite as a catalyst in reaction mechanisms that form sillimanite. *Can. Mineral.* **29**, 943-963.

_____ (1992): Forward modeling of metamorphic textures: an approach combining differential and irreversible thermodynamics. *Geol. Soc. Am., Abstr. Programs* **24**, A217.

_____ (1993): SEG93: a program to model metamorphic textures. *Geol. Soc. Am., Abstr. Programs* **25**, A264.

_____ (1994): Forward modeling of metamorphic textures: a test using polymetamorphic pelites from northwest Maine. *Geol. Soc. Am., Abstr. Programs* **26**, A-43.

_____ (1998): Domains of local reaction and their influence on nucleation in metamorphic rocks. *Geol. Soc. Am., Abstr. Programs* **30**, A-280.

_____, DUTROW, B.L. & TRAVIS, B. (1996): Simulation of metamorphic textures: combining thermal models of metamorphism with forward models of metamorphic textures. *Geol. Soc. Am., Abstr. Programs* **28**, A-424.

GUIDOTTI, C.V., CHENEY, J.T, FOSTER, C.T., HAMES, W.E., HENRY, D.J., KINNER, D.A. & LUX, D.R. (1996): Polymetamorphism in western Maine: mineralogic, petrologic and textural manifestations and regional geologic implications. *In* Guidebook to Fieldtrips in Northern New Hampshire and Adjacent Regions of Maine and Vermont (M. Van Baalen, ed.). *New England Intercollegiate Geol. Conf.* **88**, 171-202.

KRETZ, R. (1966): Grain size distribution for certain metamorphic minerals in relation to nucleation and growth. *J. Geol.* **74**, 147-173.

_____ (1969): On the spatial distribution of crystals in rocks. *Lithos* **2**, 39-66.

_____ (1973): Kinetics of crystallization of garnet at two localities near Yellowknife. *Can. Mineral.* **12**, 1-20.

_____ (1974): Some models for the rate of crystallization of garnet in metamorphic rocks. *Lithos* **7**, 123-131.

_____ (1983): Symbols for rock-forming minerals. *Am. Mineral.* **68**, 277-279.

_____ (1993): A garnet population in Yellowknife schist, Canada. *J. Metamorphic Geol.* **11**, 101-120.

_____ (1994): *Metamorphic Crystallization.* John Wiley & Sons, New York, N.Y.

RIDLEY, J. (1985): The effect of reaction enthalpy on the progress of a metamorphic reaction. *In* Metamorphic Reactions: Kinetics, Textures and Deformation (A.B. Thompson & D.C. Rubie, eds.). Springer-Verlag, Heidelberg, Germany (80-97).

SPEAR, F.S. (1988): The Gibbs method and Duhem's Theorem: the quantitative relationship among P, T, chemical potential, phase composition and reaction progress in igneous and metamorphic systems. *Contrib. Mineral. Petrol.* **99**, 249-256.

_____ (1993): *Metamorphic Phase Equilibria and Pressure–Temperature–Time Paths.* Mineralogical Society of America, Monograph **1**.

_____, KOHN, M.J. & PAETZOLD, S. (1995): Petrology of the regional sillimanite zone, west-central New Hampshire, U.S.A. with implications for the development of inverted isograds. *Am. Mineral.* **80**, 361-376.

_____, PEACOCK, S.M., KOHN, M.J., FLORENCE, F.P. & MENARD, T. (1991): Computer programs for petrologic P–T–t path calculations. *Am. Mineral.* **76**, 2009-2012.

YARDLEY, B.W.D. (1977): The nature and significance of the mechanism of sillimanite growth in the Connemara Schists, Ireland. *Contrib. Mineral. Petrol.* **65**, 53-58.

Received March 4, 1998, revised manuscript accepted March 15, 1999.

APPENDIX: CALCULATION OF LOCAL REACTIONS

The methods used to calculate reactions (1) through (23) have been discussed in detail by Foster (1981, 1982, 1983, 1986a, 1990, 1991). The procedure involves solving a set of simultaneous equations derived from: 1) Gibbs–Duhem relations that constrain the chemical potential gradients of components in local equilibrium with minerals along the transport path, 2) transport equations that link the flux of a component to its chemical potential gradient, and 3) conservation equations that link the transport of material through the region around a reaction site to the amounts of minerals precipitated or dissolved in the reaction (see Foster 1981, p. 261–264 for derivation). The equations to calculate reaction (1), sillimanite (Sil) growing in a matrix of biotite (Bt),

$$\begin{bmatrix}
\nu_{Fe}^{Bt} & \nu_{Mg}^{Bt} & \nu_{Mn}^{Bt} & \nu_{Ca}^{Bt} & \nu_{K}^{Bt} & \nu_{Na}^{Bt} & \nu_{Al}^{Bt} & \nu_{Si}^{Bt} & \nu_{H}^{Bt} & 0 & 0 & 0 & 0 & 0 \\
\nu_{Fe}^{Ms} & \nu_{Mg}^{Ms} & \nu_{Mn}^{Ms} & \nu_{Ca}^{Ms} & \nu_{K}^{Ms} & \nu_{Na}^{Ms} & \nu_{Al}^{Ms} & \nu_{Si}^{Ms} & \nu_{H}^{Ms} & 0 & 0 & 0 & 0 & 0 \\
\nu_{Fe}^{Pl} & \nu_{Mg}^{Pl} & \nu_{Mn}^{Pl} & \nu_{Ca}^{Pl} & \nu_{K}^{Pl} & \nu_{Na}^{Pl} & \nu_{Al}^{Pl} & \nu_{Si}^{Pl} & \nu_{H}^{Pl} & 0 & 0 & 0 & 0 & 0 \\
\nu_{Fe}^{Qtz} & \nu_{Mg}^{Qtz} & \nu_{Mn}^{Qtz} & \nu_{Ca}^{Qtz} & \nu_{K}^{Qtz} & \nu_{Na}^{Qtz} & \nu_{Al}^{Qtz} & \nu_{Si}^{Qtz} & \nu_{H}^{Qtz} & 0 & 0 & 0 & 0 & 0 \\
\nu_{Fe}^{Fld} & \nu_{Mg}^{Fld} & \nu_{Mn}^{Fld} & \nu_{Ca}^{Fld} & \nu_{K}^{Fld} & \nu_{Na}^{Fld} & \nu_{Al}^{Fld} & \nu_{Si}^{Fld} & \nu_{H}^{Fld} & 0 & 0 & 0 & 0 & 0 \\
L_{FeFe} & 0 & 0 & 0 & 0 & 0 & 0 & 0 & 0 & -\nu_{Fe}^{Bt} & -\nu_{Fe}^{Ms} & -\nu_{Fe}^{Pl} & -\nu_{Fe}^{Qtz} & -\nu_{Fe}^{Fld} \\
0 & L_{MgMg} & 0 & 0 & 0 & 0 & 0 & 0 & 0 & -\nu_{Mg}^{Bt} & -\nu_{Mg}^{Ms} & -\nu_{Mg}^{Pl} & -\nu_{Mg}^{Qtz} & -\nu_{Mg}^{Fld} \\
0 & 0 & L_{MnMn} & 0 & 0 & 0 & 0 & 0 & 0 & -\nu_{Mn}^{Bt} & -\nu_{Mn}^{Ms} & -\nu_{Mn}^{Pl} & -\nu_{Mn}^{Qtz} & -\nu_{Mn}^{Fld} \\
0 & 0 & 0 & L_{CaCa} & 0 & 0 & 0 & 0 & 0 & -\nu_{Ca}^{Bt} & -\nu_{Ca}^{Ms} & -\nu_{Ca}^{Pl} & -\nu_{Ca}^{Qtz} & -\nu_{Ca}^{Fld} \\
0 & 0 & 0 & 0 & L_{KK} & 0 & 0 & 0 & 0 & -\nu_{K}^{Bt} & -\nu_{K}^{Ms} & -\nu_{K}^{Pl} & -\nu_{K}^{Qtz} & -\nu_{K}^{Fld} \\
0 & 0 & 0 & 0 & 0 & L_{NaNa} & 0 & 0 & 0 & -\nu_{Na}^{Bt} & -\nu_{Na}^{Ms} & -\nu_{Na}^{Pl} & -\nu_{Na}^{Qtz} & -\nu_{Na}^{Fld} \\
0 & 0 & 0 & 0 & 0 & 0 & L_{AlAl} & 0 & 0 & -\nu_{Al}^{Bt} & -\nu_{Al}^{Ms} & -\nu_{Al}^{Pl} & -\nu_{Al}^{Qtz} & -\nu_{Al}^{Fld} \\
0 & 0 & 0 & 0 & 0 & 0 & 0 & L_{SiSi} & 0 & -\nu_{Si}^{Bt} & -\nu_{Si}^{Ms} & -\nu_{Si}^{Pl} & -\nu_{Si}^{Qtz} & -\nu_{Si}^{Fld} \\
0 & 0 & 0 & 0 & 0 & 0 & 0 & 0 & L_{HH} & -\nu_{H}^{Bt} & -\nu_{H}^{Ms} & -\nu_{H}^{Pl} & -\nu_{H}^{Qtz} & -\nu_{H}^{Fld}
\end{bmatrix}
\bullet
\begin{bmatrix}
\nabla\mu_{Fe} \bullet A/R_{Sil} \\
\nabla\mu_{Mg} \bullet A/R_{Sil} \\
\nabla\mu_{Mn} \bullet A/R_{Sil} \\
\nabla\mu_{Ca} \bullet A/R_{Sil} \\
\nabla\mu_{K} \bullet A/R_{Sil} \\
\nabla\mu_{Na} \bullet A/R_{Sil} \\
\nabla\mu_{Al} \bullet A/R_{Sil} \\
\nabla\mu_{Si} \bullet A/R_{Sil} \\
\nabla\mu_{H} \bullet A/R_{Sil} \\
R_{Bt}/R_{Sil} \\
R_{Ms}/R_{Sil} \\
R_{Pl}/R_{Sil} \\
R_{Qtz}/R_{Sil} \\
R_{Fld}/R_{Sil}
\end{bmatrix}
=
\begin{bmatrix}
0 \\ 0 \\ 0 \\ 0 \\ 0 \\
\nu_{Fe}^{Sil} \\ \nu_{Mg}^{Sil} \\ \nu_{Mn}^{Sil} \\ \nu_{Ca}^{Sil} \\ \nu_{K}^{Sil} \\ \nu_{Na}^{Sil} \\ \nu_{Al}^{Sil} \\ \nu_{Si}^{Sil} \\ \nu_{H}^{Sil}
\end{bmatrix}$$

FIG. 5. Matrix equations to solve for chemical potential gradients and reaction coefficients for reaction (1). μ_i is the chemical potential of component i in the matrix around the reaction site, μ_i^k is the amount of component i in phase k, A is the area of a surface surrounding the reaction site where the chemical potentials are measured, and R_k is the coefficient of mineral k in the reaction. The sign convention for R_k has been chosen so that R_k is positive if mineral k is produced, and negative if mineral k is consumed. L_{ii} are the straight terms in the thermodynamic diffusion coefficient matrix. Cross terms (L_{ij}, $i \neq j$) in the thermodynamic diffusion coefficient matrix were set to 0. L_{ii} were set equal for all components in this study instead of using the values determined by Foster (1981), because the effect of large changes in P and T on the L_{ii} parameters is presently unknown. Component subscripts stand for oxide components (Fe: FeO, Mg: MgO, Mn: MnO, Ca: CaO, K:$KO_{0.5}$, Na: $NaO_{0.5}$, Al: $AlO_{1.5}$, Si: SiO_2, H: H_2O).

muscovite (Ms), plagioclase (Pl), quartz (Qtz) and an H_2O grain-boundary fluid (Fld), are shown in Figure 5. The first five rows are equations derived from the Gibbs–Duhem relations for each matrix phase. These equations constrain chemical potential gradients in the matrix, provided local equilibrium is maintained. The next nine rows represent conservation equations that link the transport of components through the matrix to the net reaction inside of the region surrounded by the matrix. Gain or loss of material due to changes in concentration of components in the grain-boundary fluid (dc_i/dt) are ignored because it is several orders of magnitude smaller than the amounts of material produced or consumed by the mineral reactions (see Foster 1981, p. 262 for discussion). The first nine terms of the solution (Fig. 5, middle matrix) to this system of equations give terms ($\nabla\mu_i \cdot A/R_{Sil}$) that can be used to compare chemical potential gradients among different components that control material transport through the matrix surrounding the reaction site (see Foster 1981, p. 264 for discussion). The next five terms (R_k/R_{Sil}) give the coefficients for the reaction, normalized to the amount of sillimanite produced ($R_{sil} > 0$) or consumed ($R_{sil} < 0$) in the center of the segregation.

The coefficients of reaction (R_k) for minerals involved in reactions (1) through (23) are given in Table 3. The R_k for the seventeen reactions at the top of the table were derived by solving sets of equations like those in Figure 5 for R_k/R_p terms. The reaction stoichiometry is obtained by multiplying the R_k/R_p terms by the amount of the mineral (p) that grows ($R_p > 0$) or dissolves ($R_p < 0$) in the center of the segregation. For example, the stoichiometric coefficients (R_k) for reaction (1) were derived from the (R_k/R_{Sil}) terms in the solution to the equations shown in Figure 5 by setting $R_{Sil} = 1.0$. The resulting values are given in the first row of Table 3.

The six reactions at the bottom of the table represent situations where the overall reaction for a mechanism that dissolves a porphyroblast of staurolite or garnet splits into two parts because both the porphyroblast and some of the matrix minerals are consumed by the overall reaction. The R_k for the reaction that replaces the porphyroblast is calculated by removing the matrix minerals that are consumed by the overall reaction from the system of equations and solving for the reaction that is possible between the porphyroblast and the remaining minerals that surround it (see Foster 1991, p. 953–955 for details). If the new reaction consumes some of the remaining minerals that surround it, the minerals that are consumed by the reaction are removed from the system of equations. This process is repeated until sufficient minerals have been removed to produce a reaction that consumes the porphyroblast but has no other minerals as reactants that need to be supplied from the matrix. For example, reaction (3) was calculated in three cycles by successively removing quartz, then plagioclase, then biotite from the system of equations used to calculate reaction (2). The reaction that progresses out into the matrix is calculated by subtracting the reaction that replaces the porphyroblast from the overall reaction for the local system. For example, reaction (4) was calculated by subtracting reaction (3) from reaction (2). The staurolite for the overall mechanism of reaction is provided by reaction (3), and the quartz is provided by reaction (4). The sum of the local reactions (3 + 4) equals the overall reaction (2). In a rock with tiny, evenly distributed matrix crystals, the reaction that progresses out into the matrix (4) would split into several multiple mantles in the matrix around the porphyroblast (see Foster 1991, Fig. 5c for an example). The size of crystals in the matrix used in this paper is too large to produce well-developed multiple mantles because the thickness of the individual mantles is less than the size of the matrix crystals.

TABLE 3. STOICHIOMETRIC COEFFICIENTS FOR REACTIONS (1) THROUGH (23)

Reaction	p	R_p	R_{Bi}	R_{Ms}	R_{Pl}	R_{Qtz}	R_{Sil}^*
(1)	Sil	1.0	0.03	−0.25	−0.31	1.18	–
(2)	St	−1.0	0.44	1.92	3.22	−15.4	–
(3)	St	−1.0	–	2.01	–	–	–
(5)	Grt	1.0	−0.48	0.02	−0.68	1.62	–
(6)	St	−1.0	0.75	−0.75	0	−3.00	10.50
(7)	St	−1.0	0.21	–	–	–	8.29
(9)	Grt	−1.0	0.54	−0.54	0.05	0.80	2.05
(10)	Grt	−1.0	0.43	–	–	–	0.54
(12)	Sil	1.0	0.04	−0.27	−0.23	1.10	–
(13)	St	−1.0	0.31	2.18	2.35	−14.2	–
(14)	Grt	1.0	−0.41	−0.05	−0.47	1.17	–
(15)	Grt	−1.0	0.46	0.02	0.56	−1.44	–
(16)	Grt	−1.0	0.41	0.09	0.08	–	–
(18)	St	−1.0	0.67	−0.67	0	−2.85	10.36
(19)	St	−1.0	0.15	–	–	–	8.41
(21)	Grt	−1.0	0.53	−0.53	0.03	0.88	2.04
(22)	Grt	−1.0	0.42	–	–	–	0.56
Reaction	**method**	R_p	R_{Bi}	R_{Ms}	R_{Pl}	R_{Qtz}	R_{Sil}^*
(4)	(2) – (3)	–	0.44	−0.09	3.22	−15.4	–
(8)	(6) – (7)	–	0.54	−0.75	0	−3.00	2.21
(11)	(9) – (10)	–	0.11	−0.54	0.05	0.80	1.51
(17)	(15) – (16)	–	0.05	−0.07	0.48	−1.44	–
(20)	(18) – (19)	–	0.52	−0.67	0	−2.85	1.95
(23)	(21) – (22)	–	0.11	−0.53	0.03	0.88	1.48

The coefficients for the 17 reactions in the upper part of the table were obtained by solving matrix equations like those shown in Figure 5 as described in the text. The mineral at the center of each reaction system is given in the column labeled "p", and the amount of the central mineral that grows ($R_p > 0$) or dissolves ($R_p < 0$) is given in the column R_p. R_{Bi}, R_{Ms}, R_{Pl}, and R_{Qtz} give the moles of biotite, muscovite, plagioclase and quartz that take part in the reaction, respectively. R_{Sil}^* gives the amount of sillimanite that forms in reactons (6) to (11) and (18) to (23), where abundant nuclei of sillimanite are present in the region around staurolite or garnet porphyroblasts. The coefficients for reactions in the lower part of the table were obtained by subtracting two reactions in the upper part of the table to give the reaction for a mantle growing out into the matrix around a dissolving porphyroblast. The reactions used to calculate the mantle reactions are given in the column labeled "method". A dash means the mineral is not present.